Composites Joints Reinforced by Composites Rivets

Wenhao Li, Shijun Guo, Ioannis Giannopoulos

Centre of Aeronautics, Cranfield University, Cranfield, UK

Abstract

This paper presents an investigation into the mechanical behaviour of composite joints reinforced by using a novel composite rivet made of rolled laminates. Two typical joints have been modelled using three-dimensional solid finite element model in the study. The first type is a composites single lap joint bonded and reinforced by a composite rivet compared with the joint reinforced by a titanium bolt subjected to tensile load. The results are also compared with an adhesive bonded joint as reference. The second type of joint model is a wing box section with skin-rib joint reinforced by composite rivet subjected to a pulling load. A range of adhesive damage was modelled up to 50% (undamaged WBDM, WBDM I 16%, WBDM II 33% and WBDM III 50% respectively) of the bonding area. The results show that the rivets located in the regions where the adhesive bonding failed will carry higher stress and make more contribution to the structure integrity. Although the titanium rivets provide better mechanical performance to carry more load, composite rivets offer an alternative adequate reinforcement to delay the bonding failure and safeguard the structure.

1. Introduction

The application of fibre reinforced composites to large civil aircraft structure design is growing fast in a global scale in the last decade. It has led to increasingly interest in developing novel technologies to improve the efficiency of highly integrated composite structures. The conventional riveting and bolting techniques for metallic structures have been adopted for adhesive bonded joint of composite structures. This is partly because of the absent of ductile behaviour and damage tolerance of bonded composite joint under excessive load. Therefore, adding rivet/bolts to bonded joints is considered as a safeguard and the most efficient measure to improve the through-thickness resistant and meet airworthiness requirements.

A variety of adhesively bonded and mechanical bolted joint research has been developed to study the behaviour and in particular the failure mechanism of composites joints [1]–[4]. By adding fasteners in the bonded joint, the two joint technologies are combined to create a hybrid bonded/bolted joint which promotes the structural a higher strength. Tan investigated the efficiency of single lap joint using configurations with two and four bolts and concluded that

the load required to fracture the adhesive increased with the number of bolts. Steward et al. [5] tested single lap composite joints and concluded that bolted/bonded joint were 50% stronger than bonded/bolted joints and 16% than bonded joints. Kelly et al. studied the effect of adhesive modulus, adhesive/adherend thickness and overlap length on the load transfer in bonded/bolted CFRP single lap joints [6], [7]. It is evident that by careful material selection and joint parameter design, an appropriate load sharing between adhesive and bolt could be achieved leading to an improved strength and fatigue resistance. Guo et al. [8] investigated that the manufacturing defects reduced the strength of the adhesively bonded joint. However, many research proved that few bonded/bolted joints design experience load sharing [6], [7], [9]. The bonded/bolted joint is mainly dominated by the bonded bolted joint; after initiation of debonding the load carried by bolt increases dramatically behaving like a bolted joint. Such distinct behaviour indicate that the bolt more often acts as a safeguard to avoid catastrophic failure of bonded joints.

Since the fibre reinforced composites has superior material properties in specific direction, it has great potential to replace metal as a novel bolt to be implemented into the composites joint. This paper aims to develop a finite element model to evaluate the possibility of using the composite rivet in bonded/bolted joint instead of metal. The work was started from a single lap joint reinforced by composites and metal rivet respectively subjected to tensile load. The efficiency of the composites rivet was compared with titanium bolted-bonded composite lap-joint to evaluate their strength against pulling load. The study was then extended to a wing box section subjected to a pulling load by FE modelling and analysis. The stress in the skin-rib joint reinforced by composite rivets was analysed with the consideration of progressive adhesive damage from 16% to 50% bonding area.

2. Composite Single Lap-joint

2.1 Geometry and material properties

The dimensions of a lap-joint are shown in Fig.1. The material properties of the carbon/epoxy prepreg MTM46/HTS used for the lap-joint is presented in Table 1. Each of the laminate contains 26 plies of prepreg in a symmetrical layup $[0_4/45_3/90_3/-45_3]_s$ with a total thickness of 6.5 mm. The composites rivet is made of the same material (MTM46/HTS) in a stacking sequence of $[0_4/45_4/90_4/-45_4/0_4/45_4/-45_4]$ with a diameter of 16 mm. The longitudinal direction (0^0 direction) aligns along the rivet longitudinal axis. There is an isotropic rod of 2mm inserted and bonded in the centre of the composite rivet as shown in Fig.1 with material properties as listed in Table 2. The metallic rivet has the same dimension as the composite rivet and the same material as the isotropic rod as shown in Table 2. An adhesive layer of 0.2 mm thickness was placed between the adherends as cohesive layer following the

recommended range of experimental results summarized in Table 3 [10], where K_i is the stiffness of cohesive element, σ_i is the traction strength, G_i is the critical fracture energy release rates and i represents for n, s, t corresponded to normal, shear, tear directions.

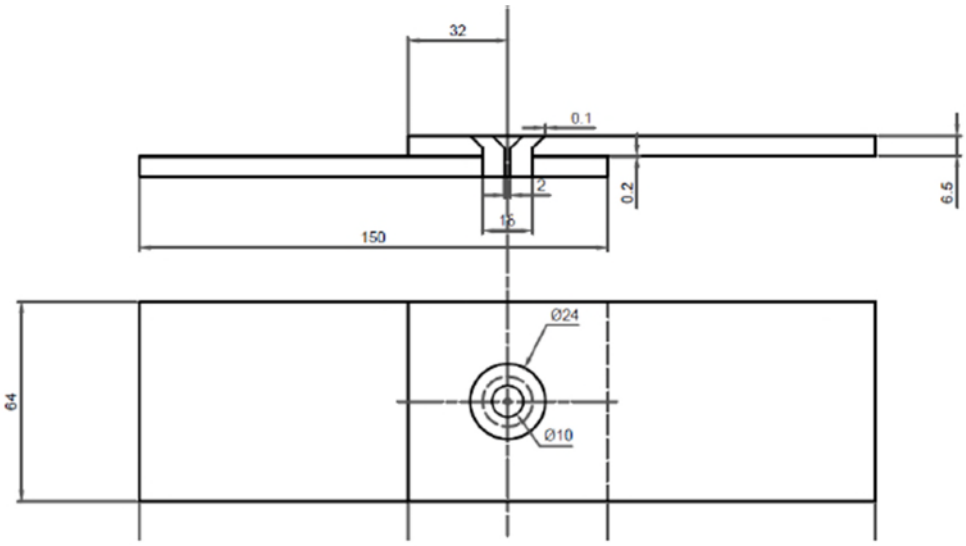

Figure 1 Single Lap joint geometry and dimension

Table 1 Material properties of carbon/epoxy prepreg (MTM46/HTS)

Carbon /epoxy MTM46/HTS	
Longitudinal modulus, $\boldsymbol{E_1}$ (GPa)	128.3
Transverse modulus, $\boldsymbol{E_2}$ (GPa)	9
In-plane shear modulus, $\boldsymbol{G_{12}}$ (GPa)	3.95
Major Poisson's ration, $\boldsymbol{\nu_{12}}$	0.32
Longitudinal tensile strength, $\boldsymbol{X_t}$ (MPa)	2278
Longitudinal compression strength, $\boldsymbol{X_c}$ (MPa)	1352
Transverse tensile strength, $\boldsymbol{Y_t}$ (MPa)	33.9
Transverse compression strength, $\boldsymbol{Y_c}$ (MPa)	210
Longitudinal shear strength, $\boldsymbol{S_{12}}$ (MPa)	98.1

Table 2 Material properties of SikaForce 7888 for adhesive layer and rod of composites rivets

	Young's Modulus (GPa)	Shear Modulus (GPa)	Poisson's Ratio
Rod	67	25.6	0.31
Adhesive	1.89	0.727	0.32

Table 3 Cohesive properties for delamination of adhesive layer

K_n	K_s	K_t	σ_n(MPa)	σ_s(MPa)	σ_t(MPa)	G_n(N/mm)	G_s(N/mm)	G_t(N/mm)
2.4E5	9.2E4	9.2E4	10	15	10	0.252	0.665	0.665

2.2 FE modelling and stress analysis

FE modelling and stress analysis of the single lap-joint reinforced by composites/metal rivet was developed by using Abaqus/standard package with non-linear stress calculation (large deformation behaviour). 3D element (C3D8R) was chosen to model the composite laminate with reduced integration and hourglass control. In order to observe the progressive damage, the 0.2 mm thickness adhesive layer between the laminates was assigned with COH3D8 element of 8 node and linear geometric order. The basic principle lying behind the progressive failure in cohesive element is the traction-separation constitutive law which assumes linear stress-displacement relationship until the initiation of the damage criterion (the quadratic nominal stress criterion employed here) followed by the degradation of the cohesive properties (mixed mode damage evolution criterion employed here) [11], [12]. The isotropic rod was modelled using 3D tetrahedron element (C3D4) with linear geometry order. In order to save computation time and assure the convergence of results, the overlap was assigned with refined mesh and the region away from bolt hole was assigned with coarser mesh, as shown in Figure 2. 8-node continuum shell elements (SC8R) was selected for composites rivet with reduced integration. The rivets was parted into 7 identical rings representing 4 layers prepreg of each ring (Figure 3). Contact between the bolt and the laminate was modelled based on the contact pair approach in Abaqus with finite sliding allowed between laminates and the bolt. A friction coefficient of 0.2 was assumed between the laminate and the bolt. The continuum mechanics approach considers a perfect bond between the adhesive and the laminate, thus, tie constraint was applied between the interface of laminates and adhesive. The left end

section of the lower composites laminate was bolted constrained and right end section of the upper composite laminate subjected to a displacement 1.5 mm in X direction, as demonstrated in Figure 4.

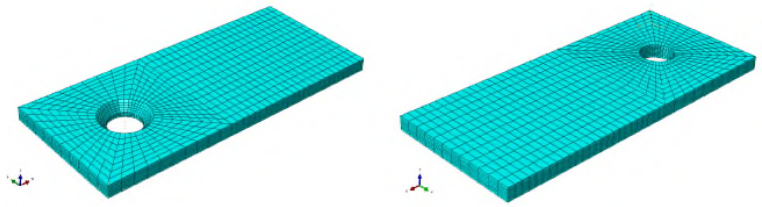

Figure 2 Mesh of the composite laminates

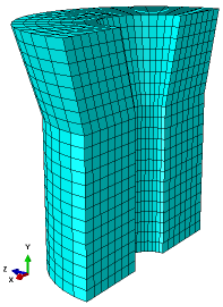

Figure 3 Mesh of rivet

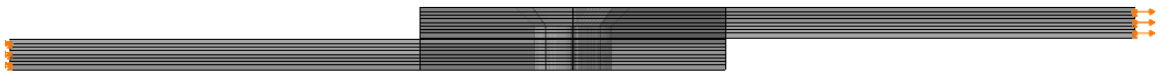

Figure 4 Boundary and loading conditions of the single-lap joint

2.3 Stress analysis and load transfer of rivet

The force-deformation results are shown in Figure 5 for the lap-joint with Composites Rivet Model (CRM), Titanium Rivet Model (TRM), Single Lap Joint bonded model (SLJ) and Single Lap Joint bonded model with the fastener hole (SLJ+H). The linear deformation of the bolted-bonded joint had the same initial variation as the baseline bonded joint. A small amount of force was carried by the rivet until a significant difference occurred, which indicates a crack in the adhesive layer and increased force transferred to the rivet. The slope disparities among CRM and TRM imply their difference in force against deflection owing to higher shear modulus of titanium than composite rivet. Observing the analogous curve of the SLJ+H, the decrease of the force carrying ability was reflected by a small gap in the SLJ curve due to the reduced bonding area of the SLJ+H with a hole of the rivet diameter.

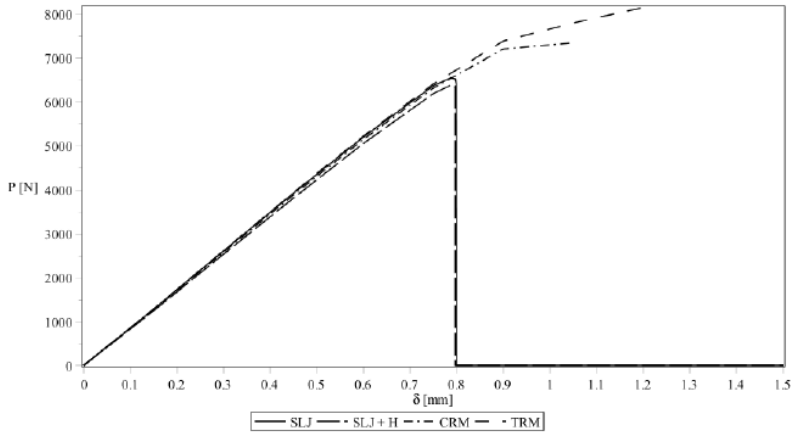

Figure 5 Force vs deformation results of bonded and bonded/bolted single lap joints

The force shared by the rivet and the adhesive layer varies in response to the propagation of progressive bonding failure. The analysis was carried out by picking the maximum σ_x in the composite rivet or the isotropic rod installed within the composite rivet. The maximum stress was obtained in different level of adhesive failure for both CRM and TRM models. The amount of stress in the interior rod reflects the ability of the rivet to carry redistributed force. It is important to note the location of the maximum σ_x during the analysis. An increase of adhesive failure amount correlates to a location of the maximum stress. Table 4 and 5 show the maximum σ_x and τ_{xz} corresponding to the respective level of adhesive failure for each model. After 95% of adhesive bonding failure, both the composite bottom plate of CRM and TRM failed in bearing mode exceeding the tensile strength 2278 MPa, which is 2356 MPa and 1927 MPa respectively as shown in Figure 6 (a) and (b). The evolution of maximum normal stress occurring in approximately the same location for both models is shown in Fig. 7 (a) and (b). For the CRM, around the maximum stress location there is a wider spreading of the stress distribution contrarily to the maximum location of the TRM.

Table 4 Maximum σ_x and τ_{xz} along the CRM rivet and the rod in different failure level

Adhesive Damage	Max. σ_x [Mpa]		Max. τ_{xz} [Mpa]	
	Rivet	**Rod**	**Rivet**	**Rod**
No Damage	13.27	12.77	7.011	1.878
Starting Damage	26.85	25.83	14.36	3.832
15 %	41.01	38.95	21.76	5.832
30 %	56.49	51.88	28.89	7.871
50 %	76.40	64.15	35.03	9.974
85 %	114.1	74.9	66.71	12.89
95 %	216.2	86.69	177.2	20.15

Table 5 Maximum σ_x and τ_{xz} along the TRM rivet and the rod with different damage level

Adhesive Damage	Max. σ_x [Mpa]		Max. τ_{xz} [Mpa]	
	Rivet	**Rod**	**Rivet**	**Rod**
No Damage	37.6	15.81	7.428	1.556
Starting Damage	76.02	32.06	15.03	3.195
15 %	116.3	48.43	23.2	4.985
30 %	160.6	64.69	32.84	7.114
50 %	215.9	80.56	46.49	10.14
80 %	303.7	96.28	77.01	16.27
90 %	512.2	120.9	207.7	35.85
95 %	778	142	350.5	56.69

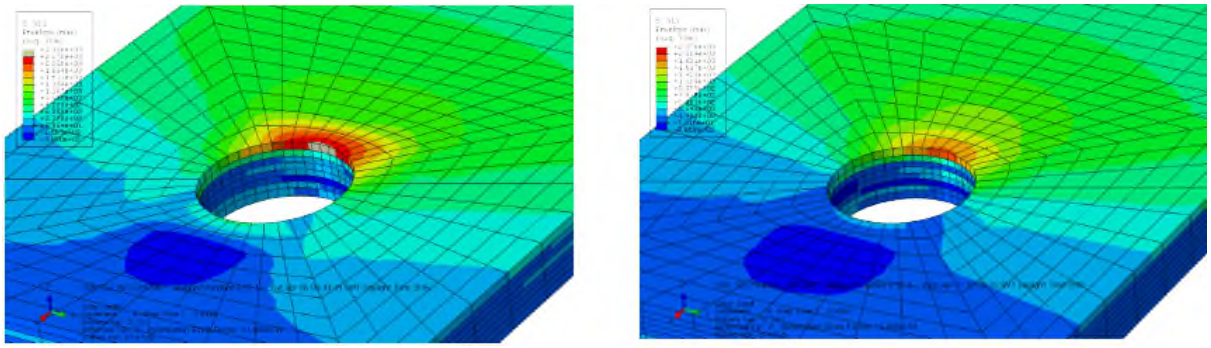

(a) Composites rivet model *(b) Titanium rivet model*

Figure 6 σ_x distribution loaded at 1.05 mm

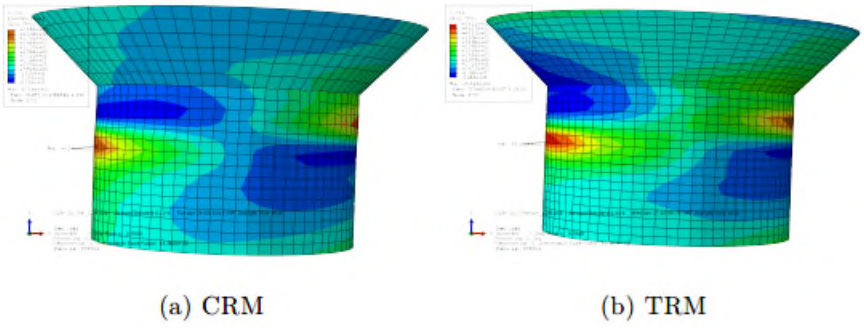

Figure 7 Tensile stress distribution of the rivets for both models

The maximum σ_x and τ_{xy}in the rivets and rod for the two models is plotted in function of the joint deformation as shown in Figure 8 and Figure 9.

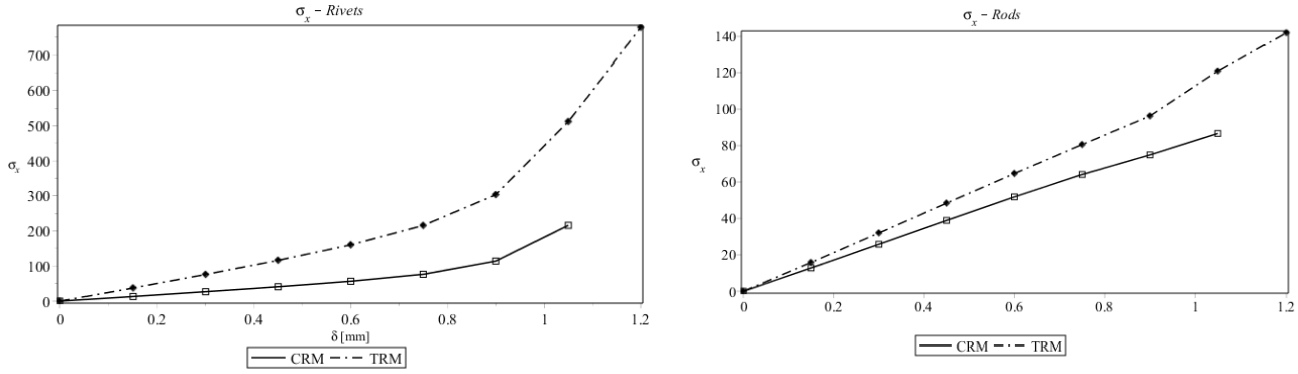

(a) Rivet *(b) Rod*

Figure 8 Maximum σ_x on rivets/rod versus applied displacement

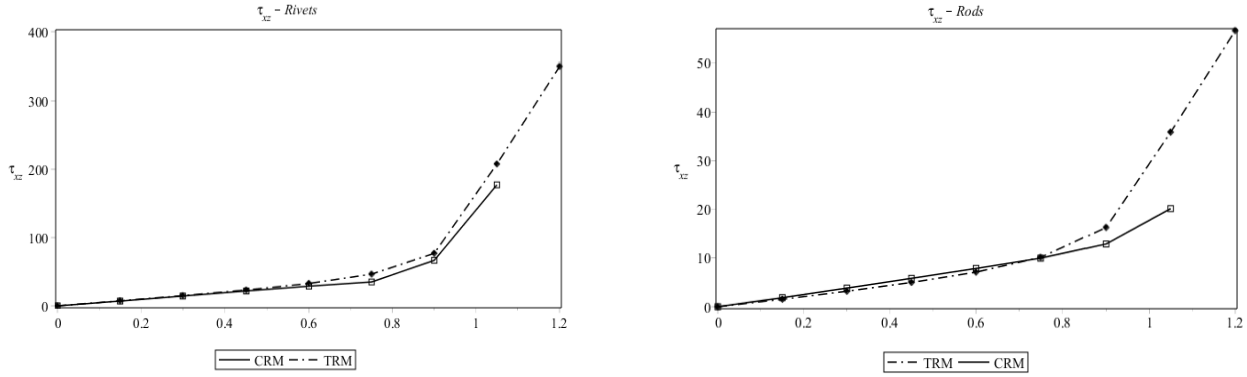

(c) Rivet *(d) Rod*

Figure 9 Maximum τ_{xy} on rivet/rod versus applied displacement

At $\delta = 0.9$ mm from the plots of figure 8 and 9, a drastic increase of the stress is noticeable corresponding to decrease of the force at the point as shown in figure 5. Both models are

subjected to this sudden increase of stress. It indicates a severe adhesive failure occurring at this force level for both models. In response to the initial bonding failure, more force would be transferred to the rivets. The titanium rivet of larger G value could offer better reinforcement with a delayed failure through the adhesive in particular the rivet pull-out in the final joint failure phase. On the other hand, although the composite rivet of smaller G results in slightly larger shear stress in the adhesive layer, the progressive failure rate of the joint reinforced by composite rivet is competitive to the titanium rivet. While the final rivet pull-out following the complete failure of adhesive layer is beyond the main concern of the study.

3. Wing box section model

The earlier study results have demonstrated sufficient reinforcement for lap-joint by using composites rivet, which is even comparable to metal rivet. The study is extended to investigation into a composite wing skin-rib joint structure reinforced by composite rivets. In this FE model as shown in Figure 10, a row of 6 rivets is employed to reinforce the bonded joint for the wing box assembly. Figure 11 shows one of the drilled countersunk holes on the upper skin, which is bonded to the rib flange using adhesive layer. The rib web is reinforced by 14 vertical stiffeners.

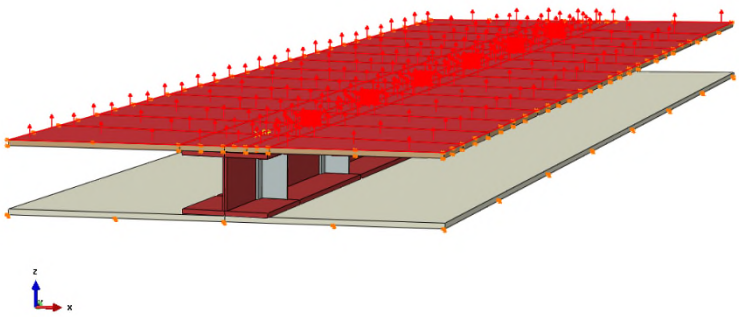

Figure 10 Assembly of the wing box section

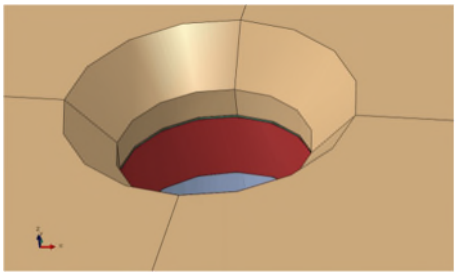

Figure 81 Example of a drilled hole into the structure

3.1 Material Properties

The material of the skins, stiffeners and the rib are made of aluminium since it is one of the most commonly used materials for this type of structures (Young's modulus of 72 GPa and Possion's ratio of 0.27). The adhesive layer is made by the ductile SikaForce 7888 and was modelled as an isotropic material, as presented in Table 2. The washer located on the bottom of each composite rivet is made of composite material of the same properties. The material and the laminated stacking sequence of the composite rivets are the same as the sing lap-

joint panel in the earlier example. The isotropic rod placed in the composite rivet centre remains the same as that in the lap-joint rivet.

3.2 Loads and interactions

The bottom skin of the structure was perfectly connected to the rib's lower surface through a tie constraint from Abaqus. The 14 stiffeners of the rib web of equal pitch were tied to the rib web on both side surfaces. The bonding interfaces between adherend and adhesive layer were modelled using tie constraint in Abaqus. The upper and lower face of the adhesive layer was bonded to the lower surface of the upper skin and the upper surface of the rib flange respectively.

The contact between the composite rivet and respective hole was modelled in surface-to-surface contact based on a master-slave concept. The finite sliding formulation was chosen. In this model, the possible contact between master and slave nodes is defined at the beginning of the analysis and continuously redefined during the analysis process. This model ensures a convergent solution either for small sliding or significant sliding. In this case the picked master surface is the hole internal surface plus the adhesive surface and the slave surface to match the exterior surface of the rivet. Similarly the contact between the washer and the lower face of the rib upper flange was modelled using the same surface-to-surface contact model. A friction coefficient between all the contacting surfaces was 0.2. In the analysis, a pressure of 27450 Pa normal to the skin surface was applied to the model as illustrated in Figure 10 to represent aerodynamic force. The displacement along the edge of the upper and lower skins and stiffeners were constrained in X and Y direction with freedom in rotations.

3.3 Mesh of the FE model

All parts of the skin-rib FE model were meshed using 3D brick elements (C3D8R in Abaqus). The 3D element is of 8 node-brick with linear geometric order and reduced integration with hourglass control. The regions of the upper skin and the adhesive layer closest to the rivet holes were modelled using a higher mesh density than the remaining regions. Around the holes the mesh is further refined. Since the stress analysis was focused on the upper skin joint, the lower skin model has a coarser mesh for all the remaining parts. The mesh refinement is illustrated on Figure 12 as an example of the WBDM I model. For this example, the behaviour and load carrying ability of each rivet are studied in 4 different level of adhesive layer failure in the joint as shown in Figure 13 and Table 6.

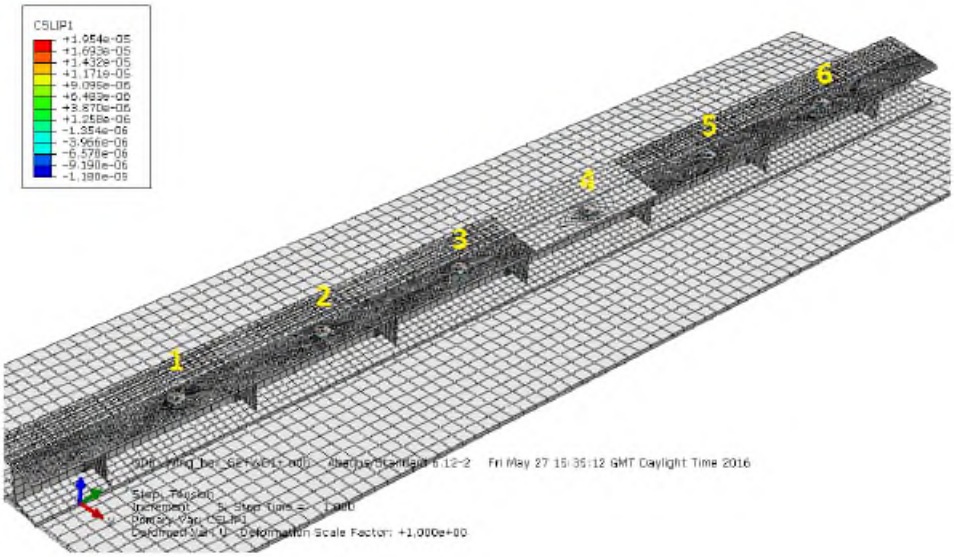

Figure 12 Mesh refinements of WBDM I

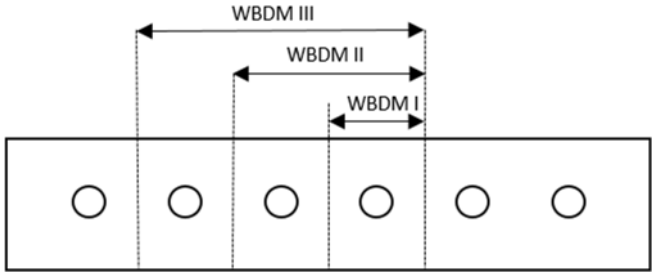

Figure 13 Damage Level of Adhesive Layer

Table 6 Damage level

WBDM	No damage
WBDM I	16% damage
WBDM II	25% damage
WBDM III	50% damage

3.4 Stress distributions in the joint

The pressure applied to the upper skin results in a bending associated with vertical displacement of the structure. For a case of bonding failure between the skin and rib flange, the local deformation will occur as shown in Figure 14 based on the model WBDM III. The results are presented in Figure 15 (a~d). It is noticed that the maximum stress of rivet located in the bonding failure region is much higher than that in the bonded regions. The stress level transferred to those rivets is much higher than the adhesive strength. According to these results a wing box joint with only adhesive bonding will not be able to withstand this level of loading and stress. For this application, the use of rivets to reinforce the joint and improve damage tolerance of the wing box joint is vital. On the other hand the rivets near the bonding failure boundary are critical. As the failure region increases, the maximum tensile stresses of those rivets are increasing and carry higher stress to slow down the crack propagation.

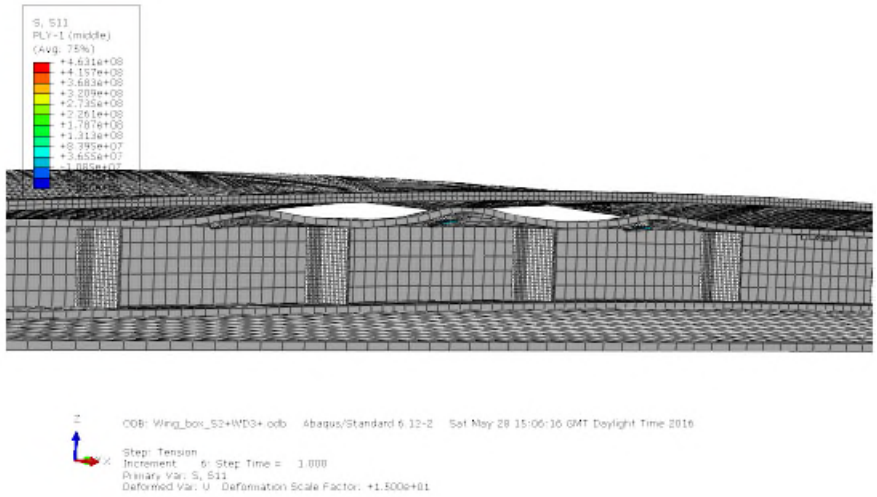

Figure 14 Structural behaviour of WBDM III under the applied pressure

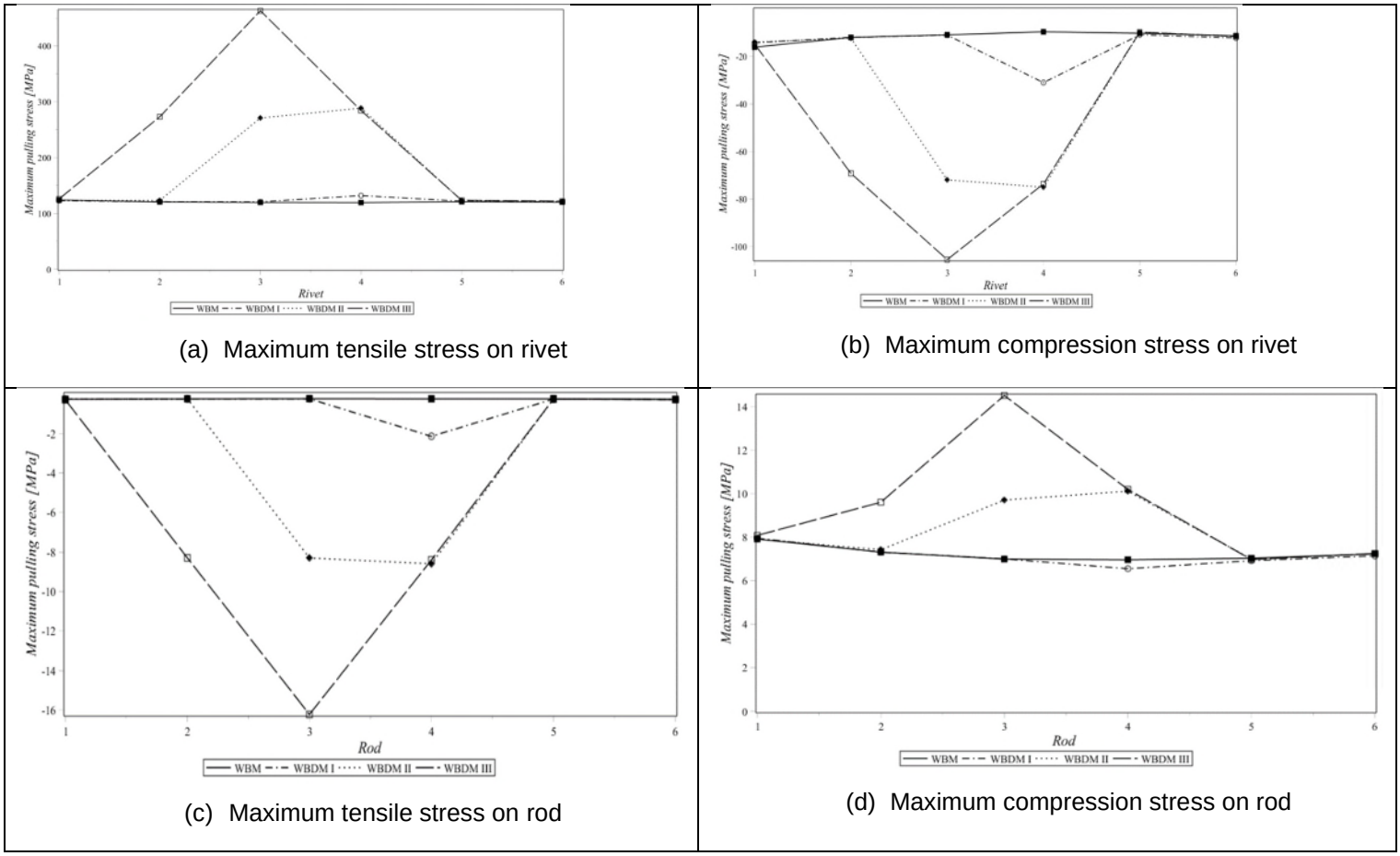

(a) Maximum tensile stress on rivet

(b) Maximum compression stress on rivet

(c) Maximum tensile stress on rod

(d) Maximum compression stress on rod

Figure 15 Maximum tensile/compression stress on rivet/rod surface for each level of adhesive damage

4. Conclusion:

The proposed composite rivet offers an alternative solution for structure joint reinforcement through-thickness to the conventional metallic rivet. Comparing with titanium rivet, the composite rivet of the same dimension demonstrates a competitive strength with almost the same stress variation trend.

The study on a composite single lap-joint subjected to tension shows that the stress carried by the fastener is small until the adhesive failure starts. After an initial bonding crack, the composite rivet plays a more important role to prevent undesirable sudden failure. The study on a wing box skin-rib joint reinforced by using a raw of composite rivets also demonstrated the same structural behaviour. The rivets play a role of debonding barrier by carrying significantly higher tress to slow down the bonding crack propagation after initial failure. The rivets close to the bonding failure region provide a means to increase damage tolerance and structure integrity of the jointed structure.

Acknowledgments

The authors acknowledge the financial support from China Scholarship Council (CSC NO. 201708140099) and BAE Systems.

Reference:

[1] W. D. Nelson, B. L. Bunin, and L. J. Hart-Smith, “Critical Joints in Large Composite Aircraft Structure.,” MCDONNELL DOUGLAS CORP LONG BEACH CA DOUGLAS AIRCRAFT DIV, 1983.

[2] L. J. Hart-Smith, “Analysis and design of advanced composite bounded joints,” 1974.

[3] L. J. Hart-Smith, “Bolted Joints In Graphite-Epoxy Composites.,” MCDONNELL DOUGLAS CORP LONG BEACH CA DOUGLAS AIRCRAFT DIV, 1976.

[4] E. W. Thrall Jr, “Primary adhesively bonded structure technology (PABST),” *J. Aircr.*, vol. 14, no. 6, pp. 588–594, 1977.

[5] M. Stewart and M. Stewart, “An experimental investigation of composite bonded and/or bolted repairs using single lap joint designs,” in *38th Structures, Structural Dynamics, and Materials Conference*, 1997, p. 1339.

[6] G. Kelly, “Quasi-static strength and fatigue life of hybrid (bonded/bolted) composite single-lap joints,” *Compos. Struct.*, vol. 72, no. 1, pp. 119–129, 2006.

[7] G. Kelly, “Load transfer in hybrid (bonded/bolted) composite single-lap joints,”

Compos. Struct., vol. 69, no. 1, pp. 35–43, 2005.

[8] S. Guo and R. Morishima, “Numerical analysis and experiment of composite sandwich T-joints subjected to pulling load,” *Compos. Struct.*, vol. 94, no. 1, pp. 229–238, 2011.

[9] J. H. Kweon, J. W. Jung, T. H. Kim, J. H. Choi, and D. H. Kim, “Failure of carbon composite-to-aluminum joints with combined mechanical fastening and adhesive bonding,” *Compos. Struct.*, vol. 75, no. 1–4, pp. 192–198, 2006.

[10] H. Cui, Y. Li, Y. Liu, J. Guo, and Q. Xu, *Numerical simulation of composites joints failure based on cohesive zone model*, vol. 27. 2010.

[11] Z. Hashin and A. Rotem, “A fatigue failure criterion for fiber reinforced materials,” *J. Compos. Mater.*, vol. 7, no. 4, pp. 448–464, 1973.

[12] Z. Hashin, “Failure criteria for unidirectional fiber composites,” *J. Appl. Mech.*, vol. 47, no. 2, pp. 329–334, 1980.

2018-05-08

Composites joints reinforced by composite rivets

Li, Wenhao

Asranet, Glasgow

Li W, Guo S, Giannopoulos I. (2018) Composites joints reinforced by composite rivets. In: 1st International Conference on Advances in Aerospace Structures, Systems and Technology: AASST, 6-8 May 2018, London, UK

https://dspace.lib.cranfield.ac.uk/handle/1826/17194